Integrated optical Dirac physics via inversion symmetry breaking

Matthew J. Collins, Fan Zhang, Richard Bojko, Lukas Chrostowski, and Mikael C. Rechtsman

Phys. Rev. A **94**, 063827 — Published 13 December 2016

DOI: 10.1103/PhysRevA.94.063827

Integrated optical Dirac physics via inversion symmetry breaking

Matthew J. Collins[1], Jack Zhang[2], Richard Bojko[3], Lukas Chrostowski[2], and Mikael C. Rechtsman[1]

[1]*Physics Department, the Pennsylvania State University, University Park, PA 16802*
[2]*Department of Electrical and Computer Engineering, University of British Columbia 2332 Main Mall, Vancouver V6T 1Z4 Canada*
[3]*Department of Electrical Engineering, University of Washington, Seattle, WA 98195 USA*

Abstract: Graphene and boron nitride are two-dimensional materials whose atoms are arranged in a honeycomb lattice. Their unique properties arise because their electrons behave like relativistic particles (without and with mass, respectively) – namely, they obey the Dirac equation. Here, we use a photonic analogue of boron nitride to observe Dirac physics in a silicon integrated optical platform. This will allow for photonic applications of Dirac dispersions (gapped and ungapped) to be realized in an on-chip, integrated nanophotonic platform.

There has been a great deal of recent interest in the photonic analogue of graphene – specifically, photonic structures wherein light (as opposed to electrons) obeys the Dirac equation. The first realization of photonic graphene[1] was in a photorefractive crystal with an optically induced honeycomb lattice refractive index profile, and was used to observe conical diffraction[2]. Since then, there has been a wide variety of photonic and polaritonic systems that exhibit Dirac physics. They include honeycomb lattices of direct-laser-written waveguides in fused silica[3–6]; microwave photonic crystals[7], macroscopic photonic crystals[8]; coupled microwave resonators[9,10]; nonlinear photorefractive crystals[11]; quantum well micropillar honeycomb lattices that exhibit exciton-polaritons with Dirac dispersion[12]. Moreover, Dirac physics has been probed in other wave-based systems[13] such as in ultracold fermions[14], electrons in quantum well structures[15], as well as in molecular complexes[16].

To date, photonic graphene has enabled the observation of a number of new physical effects such as exceptional-point rings[8] for use in efficient high-power large-area lasers, strain-induced pseudomagnetism[3]; photonic topological insulators[5]; and the prediction[17] and observation[4] of topological transitions; among others. There are a number of other proposed technological implications of realization Dirac physics for photons, including effective epsilon-near-zero materials for transformation optics applications[7,18,19], the realization of large-area high-power single-mode diode lasers[20–22], the realization of robust photon transport in planar photonic topological insulators[23–26], and valley Hall photonic topological insulators[27] (more below on these applications). However, to date there has been no realization of photonic Dirac behavior in an integrated optics platform, for use in optical devices. Perhaps the reason for this is that a Dirac *cone* (i.e., the massless particle case) has no associated band gap. As a result, when light is passed through the structure with a Dirac cone in transmission experiments, there is no clearly observable spectral signature. This is in contrast to reflection experiments on large-area photonic crystals[8]; or fluorescence measurements in exciton-polariton systems[12], for example, which permit direction observation of the Dirac spectrum via leaky modes above the light line.

Here, we demonstrate a photonic analog of boron nitride in a silicon photonic crystal slab. The experimental signature of the Dirac dispersion is a band gap that opens as the inversion symmetry is broken for the graphene-like honeycomb photonic crystal. Moreover, the associated Dirac cone is not 'accidental'[7,8] – it robustly arises from the hexagonal symmetry of the structure without any need for fine-tuning. Samples of increasing inversion symmetry breaking were fabricated to realize the transition between photonic graphene and photonic boron nitride. We probed the band gaps using broadband optical transmission measurements.

Using inversion symmetry breaking, we can open a photonic band gap exhibiting a Dirac cone, thus turning a realization of photonic graphene into 'photonic boron nitride'. The opening of a band gap as a result of broken inversion symmetry is a hallmark property of the honeycomb lattice[28]. The Dirac equation and its associated dispersion can be written as follows:

$$i\partial_t \begin{pmatrix} \psi_1 \\ \psi_2 \end{pmatrix} = v \begin{pmatrix} m & i\partial_x + \partial_y \\ i\partial_x - \partial_y & -m \end{pmatrix} \begin{pmatrix} \psi_1 \\ \psi_2 \end{pmatrix} \rightarrow E = \pm v\sqrt{|\boldsymbol{k}|^2 + m^2},$$

where i is the square root of -1, t is time, ψ_1 and ψ_2 are the wavefunction components; v is the maximum velocity (also called Fermi velocity) of the particle; m is the mass of the particle in question, E is the particle's energy, and $\boldsymbol{k}$ is its momentum. Note that for $m=0$, the dispersion relation $E(\boldsymbol{k})$ describes a cone, and for $m\neq 0$, it describes two hyperbolae with a gap in between of size $2m$.

The photonic system used here is composed of a photonic crystal in a silicon-on-insulator (SOI) platform. A honeycomb lattice of holes (each *114nm* in radius, nearest-neighbor spacing *273nm,* lattice constant *a=473nm*) is fabricated on a silicon chip (*220nm* thick, refractive index 3.48 at wavelength 1550nm), clad on both sides by silica (refractive index 1.44 at 1550nm). A scanning-electron-microscope (SEM) image of the design is shown in Fig. 1(a). The associated photonic band structure simulation for the transverse-electric-like (TE) polarization is shown in Fig. 1(b): note the presence of the touching point between the first and second bands, at the Brillouin zone vertex (*K*-point). Viewed as a full two-dimensional dispersion, this point is a Dirac cone, whereby photons obey the Dirac equation (see inset conical dispersion). Note that the dispersion shown is based on a photonic crystal slab calculation (using a full three-dimensional simulation to incorporate the finite height of the slab embedded in the silica cladding), as opposed to a purely two-dimensional system. Numerical calculations of the band structure are performed using the MIT-Photonic-Bands (MPB) software package[29].

In order to induce a band gap, we break inversion symmetry by giving the two distinct honeycomb sublattices different hole radii. For example, in Fig. 1(c), we show a SEM image of the fabricated structure with hole radii $r_1=100nm$ and $r_2=128nm$ for the two sublattices. The associated TE photonic band structure is shown in Fig. 1(d): here, a band gap has opened at the Dirac point. The band gap size is directly proportional to the strength of inversion symmetry breaking; specifically, the difference in radii between the holes in the two sublattices.

We perform transmission experiments through the structure in order to directly observe the opening of the band gap as a function of increasing symmetry breaking. Light is coupled into the

silicon chip using highly efficient grating couplers[30], passed through a photonic crystal of length *47μm* along the transmission direction and *24μm* wide in the transverse direction. The design of the device is shown in Fig. 1(e). A swept telecommunications-band laser system (Agilent 8164A) is used to inject TE-polarized light into the input grating coupler using standard single mode silica fiber. Light is then out-coupled from a second grating and the transmission is then measured as a function of wavelength across a bandwidth range 100nm centered on 1550nm.

The photonic band gap is directly observable because there are no extended Bloch states therein; therefore transmission through the structure goes to zero. An example of a transmission experiment is shown in Fig. 2, including calculated band structure and corresponding transmission spectrum. In Fig. 2(a), the band structure exhibits a TE band gap (blue curves) due to inversion breaking (this corresponds to the case of Fig. 1(c)). The red-dashed curves show the case where the hole radii are the same, therefore there is no band gap. The blue area is the light cone region, which contains states that reside both within the slab and outside it in the cladding; these are radiative states that make only a small contribution to the transmission. Indeed, most such states reside almost entirely outside the slab (except for potential slab resonances[31]). The transmission experiment for the inversion symmetry broken photonic boron nitride is shown in Fig. 2(b). Clearly, there is a dramatic drop in transmission (~40dB) within the band gap induced by inversion symmetry breaking.

Another feature appearing in the band structure is an increase in transmission followed by a drop that is less steep than that of the band gap (see black dashed line in Fig. 2(b)). This feature can be interpreted as an increase in density-of-states at the band 'shoulder' (a local maximum of the second band - see label in Fig. 2(a)), leading to higher transmission. At frequencies above the shoulder, there are significantly fewer states, therefore there is a drop in transmission. The position of the band shoulder relative to the band gap edges can be further used to characterize the photonic bands experimentally.

We note that the second band has a lower frequency at the M-point than at the K-point (where the Dirac regime resides), as can be seen clearly in Fig. 2(a). This is true regardless of whether $\Delta r=0$ or otherwise (i.e., whether the Dirac dispersion is massless or massive). This is not the case in solid-state graphene or boron nitride: in those cases, the second band lifts above and resides well away from the Dirac region by the time it gets to the M-point. The reason for this difference is that a photonic crystal slab is not composed of localized orbitals largely confined to individual atoms (with corresponding hopping amplitudes to tunnel from one atom in the lattice to the next), like two-dimensional materials. Rather, it is described by a Helmholtz equation that has no bound states due to the positivity of the Maxwell operator[32].

We fabricated a number of photonic crystal slab structures with different amounts of inversion breaking, ranging from $\Delta r=0$ through $\Delta r=30nm$. In Fig. 3, we plot two quantities: the size of the band gap (in blue), and the frequency separation between the bottom of the band gap and the second band shoulder (in red), both as a function of Δr. Experimental results are depicted by dots and numerical calculations by solid lines: clearly there is good agreement between these. The slight systematic underestimate of the band gap by the numerical simulation likely arises in part due to the uncertainty in the position of the drop-off of transmission. Note that only relative quantities are plotted here (rather than absolute frequencies) due to a roughly 10-20nm

wavelength shift of the observed spectra from numerically predicted values (this is typical in silicon photonics[33]), and here is most likely due to possible thickness and hole size differences (the sensitivity of the Dirac point frequency to fabrication variations is 2.4 $x10^{-4}$(c/a)/nm in thickness, and $1.4x10^{-3}$(c/a)/nm in hole radius). This accounts for the difference in the vertical axes in Fig. 2(a) and Fig. 2(b). Figure 3 clearly shows that the band gap opens at non-zero inversion breaking. The origin of this is the decrease of the second band at the M-point, as discussed above. Although a gap opens locally at the Dirac point for any nonzero Δr, the second band does not lift out of the way until finite Δr. This likely also accounts for the overestimate of the band gap for small Δr: a sharp decrease in density-of-states associated with the lifting of the Dirac cone gives rise to a drop in transmission despite the lack of a complete band gap.

The decrease in the second band at the M-point obscures the Dirac region; however, this does not negate a number of potential applications of photonic Dirac physics. These include the presence of flat-band slow-light edge modes for Purcell-enhancement applications[34] (these only require a band gap at a given lattice momentum parallel to the edge), as well as achieving a topological band gap[26], among others. Moreover, the presence of an obscuring band in the context of this experiment is moot because the Dirac cone by itself would in any case not be observable in transmission experiments due to a lack of a band gap. That said, when the dielectric contrast between the phases is increased (beyond the presently used 3.47:1.44), the second band lifts at the M-point and the Dirac dispersion is unobscured by other bands. An obvious route to achieve this would be to clad both sides of the silicon slab by air, rather than silica, by performing an under-etch of the structure. In the present structure, however, since inversion breaking lifts the second band at both the M and K points, the band gap is directly observable.

Before concluding, we discuss the specifics on potential applications of having a Dirac dispersion in a photonic band structure. One is the possibility of achieving large-area single-mode photonic crystal semiconductor lasers. The motivation behind this active research field[35] is that if laser gain is distributed over large areas, higher powers can be achieved. Due to the unique density-of-states profile associated with Dirac cones (it goes linearly to zero at the Dirac point) macro-scale potentially lasing Bloch modes are spaced as far away from one another as possible in frequency. Therefore, single-mode lasing would be possible in over areas where multimode behavior (thus with an irregular spatial mode profile) would be the norm[20]. Dirac cones lying under the light line (as realized here) would therefore give rise to high-power in-plane lasing, exploiting the large area of the photonic crystal. Yet another application related to large-area light-matter coupling is that of realizing *Landau levels*[3]. Originally associated with the quantum Hall effect[36], these are highly degenerate energy levels that can arise from inhomogeneous (i.e., aperiodic) strain of a lattice with Dirac cones[37,38]. High degeneracy means high density-of-states, and therefore increased light-matter coupling – for example in coupling photonic crystals to quantum dots for quantum information applications[39], or enhanced nonlinear optics[40]. This brings up a fascinating question: can aperiodic photonic crystals achieve higher density-of-states than periodic ones? Yet another application is dispersion engineering for various transformation optics applications, including cloaking[7], and epsilon-near-zero materials[18,41]. A Dirac cone is associated with zero-index behavior in a non-resonant (and therefore in principle loss-free) device. Finally, the presence of Dirac cones is a precursor to the realization of a photonic topological insulator – in fact, it represents a transition point between topological and trivial band gaps. A number of theoretical proposals have utilized this to realize

topological behavior[23,26,42], with experimental realizations in various contexts including condensed matter physics[43,44], cold atomic gases[45], optical waveguide arrays[5], and microwave photonics[46,47]. The realization of a photonic-crystal-based topological insulator[48] would enable highly robust nanophotonic edge channels – at the smallest scale possible for a low-loss optical device.

In summary, we have demonstrated Dirac physics in an integrated silicon photonic platform. The Dirac dispersion behavior was observed by breaking the inversion symmetry of the structure by allowing the different sublattices of a honeycomb photonic crystal slab to have different hole radii. This opened a band gap (a photonic equivalent to the electronic band gap of the semiconductor boron nitride), which was directly observable in transmission experiments. The photonic crystal slab geometry that was utilized allows for complete guidance of light without leakage, making it suitable for use in integrated optical devices. The observation of photonic Dirac physics in silicon photonics can enable a range of unconventional optical devices.

Acknowledgements: The devices were fabricated at the Washington Nanofabrication Facility (WNF) at the University of Washington, part of the National Science Foundation National Nanotechnology Infrastructure Network (NNIN). We also acknowledge the support of Prof. N. Jaeger.

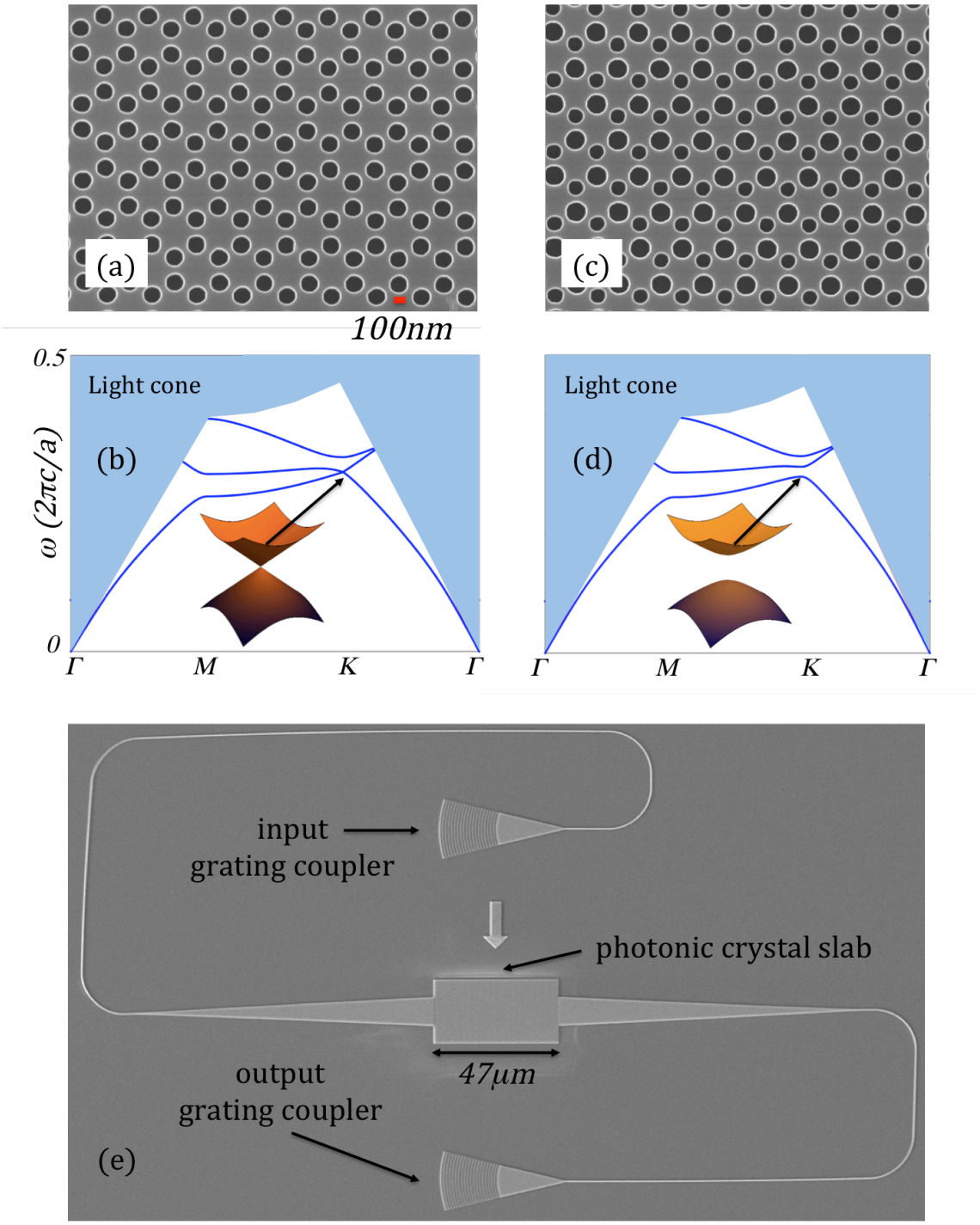

Figure 1. (a) SEM image of honeycomb lattice photonic crystal slab structure (holes are *114nm* in radius, nearest-neighbor spacing *273nm,* lattice constant *a=473nm,* slab height *220nm*), with corresponding photonic band structure shown in (b). (c) Same as (a), but with an inversion broken: the holes of the two triangular sublattices have different radii, (*Δr=27nm*), with corresponding photonic band structure shown in (d). (e) is an SEM image of the entire device, including grating couplers.

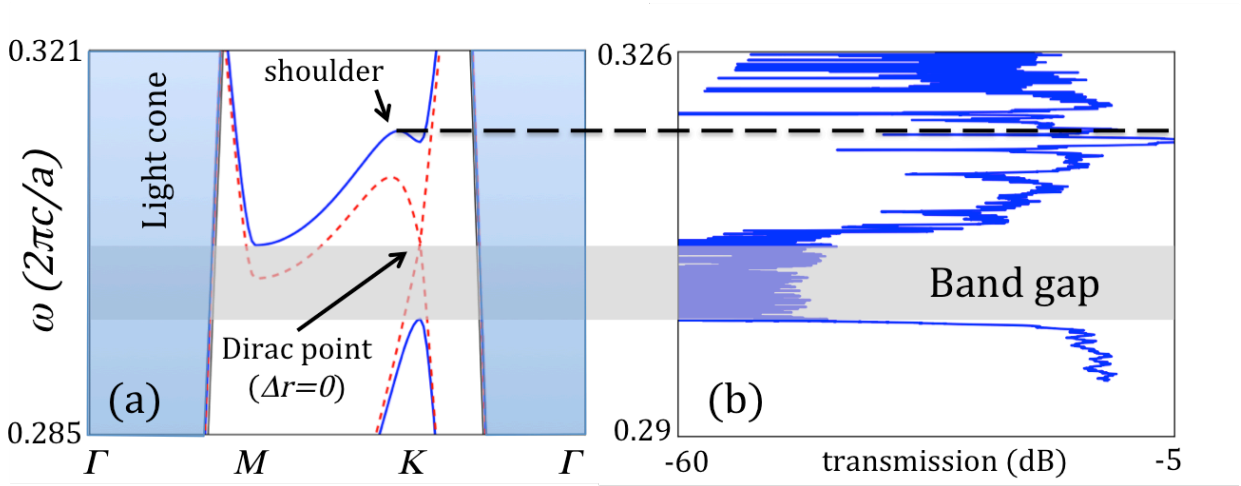

Figure 2. (a) Dispersion diagram (band structure) for the inversion-symmetry-broken photonic crystal slab shown in Fig. 1(c) (difference in hole radius $\Delta r=27nm$, blue solid line), and that without inversion breaking, and thus still a Dirac cone (red dashed line). (b) Experimental results for the transmission through the inversion-broken structure. The band gap is clearly observed as a sharp decrease in transmission. The black dashed line indicates the second band 'shoulder', where an increase and then sharp decrease in density-of-states leads to a peak in transmission.

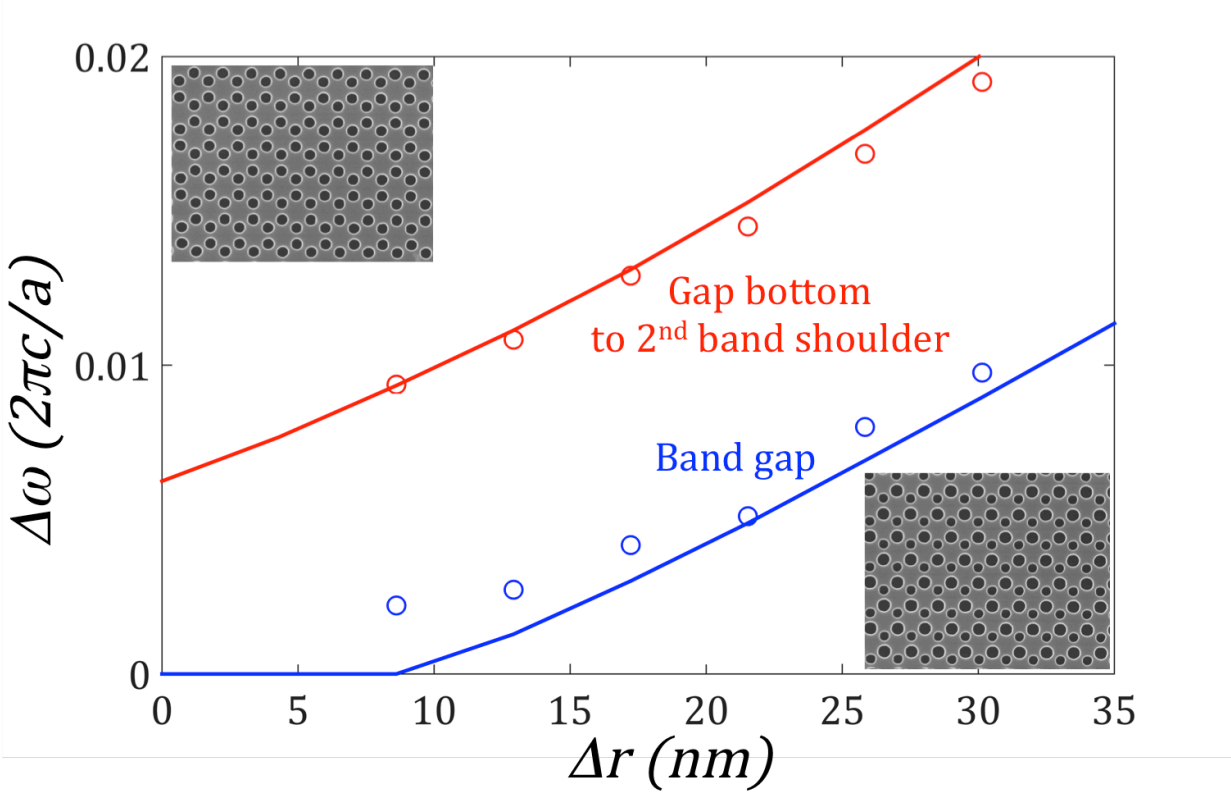

Figure 3. Plot of the band gap size (blue) and frequency difference between the bottom of the band gap and the second band shoulder (red). Experimental results are shown as circles and numerical calculations are solid curves. Inset are SEM images of the photonic crystal structures at $\Delta r=0$ (at left) and $\Delta r=27nm$ (at right).

References

1. Peleg, O. *et al.* Conical Diffraction and Gap Solitons in Honeycomb Photonic Lattices. *Phys. Rev. Lett.* **98,** 103901 (2007).

2. Berry, M. V., Jeffrey, M. R. & Lunney, J. G. Conical diffraction: observations and theory. *Proc. R. Soc. Math. Phys. Eng. Sci.* **462,** 1629–1642 (2006).

3. Rechtsman, M. C. *et al.* Strain-induced pseudomagnetic field and photonic Landau levels in dielectric structures. *Nat. Photonics* **7,** 153–158 (2013).

4. Rechtsman, M. C. *et al.* Topological Creation and Destruction of Edge States in Photonic Graphene. *Phys. Rev. Lett.* **111,** 103901 (2013).

5. Rechtsman, M. C. *et al.* Photonic Floquet topological insulators. *Nature* **496,** 196–200 (2013).
6. Plotnik, Y. *et al.* Observation of unconventional edge states in 'photonic graphene'. *Nat. Mater.* **13,** 57–62 (2014).
7. Huang, X., Lai, Y., Hang, Z. H., Zheng, H. & Chan, C. T. Dirac cones induced by accidental degeneracy in photonic crystals and zero-refractive-index materials. *Nat. Mater.* **10,** 582–586 (2011).
8. Zhen, B. *et al.* Spawning rings of exceptional points out of Dirac cones. *Nature* **525,** 354–358 (2015).
9. Kuhl, U. *et al.* Dirac point and edge states in a microwave realization of tight-binding graphene-like structures. *Phys. Rev. B* **82,** 94308 (2010).
10. Bellec, M., Kuhl, U., Montambaux, G. & Mortessagne, F. Topological Transition of Dirac Points in a Microwave Experiment. *Phys. Rev. Lett.* **110,** 33902 (2013).
11. Song, D. *et al.* Unveiling pseudospin and angular momentum in photonic graphene. *Nat. Commun.* **6,** 6272 (2015).
12. Jacqmin, T. *et al.* Direct Observation of Dirac Cones and a Flatband in a Honeycomb Lattice for Polaritons. *Phys. Rev. Lett.* **112,** 116402 (2014).
13. Polini, M., Guinea, F., Lewenstein, M., Manoharan, H. C. & Pellegrini, V. Artificial honeycomb lattices for electrons, atoms and photons. *Nat. Nanotechnol.* **8,** 625–633 (2013).
14. Tarruell, L., Greif, D., Uehlinger, T., Jotzu, G. & Esslinger, T. Creating, moving and merging Dirac points with a Fermi gas in a tunable honeycomb lattice. *Nature* **483,** 302–305 (2012).

15. Singha, A. *et al.* Two-Dimensional Mott-Hubbard Electrons in an Artificial Honeycomb Lattice. *Science* **332,** 1176–1179 (2011).
16. Gomes, K. K., Mar, W., Ko, W., Guinea, F. & Manoharan, H. C. Designer Dirac fermions and topological phases in molecular graphene. *Nature* **483,** 306–310 (2012).
17. Delplace, P., Ullmo, D. & Montambaux, G. Zak phase and the existence of edge states in graphene. *Phys. Rev. B* **84,** 195452 (2011).
18. Alù, A., Silveirinha, M. G., Salandrino, A. & Engheta, N. Epsilon-near-zero metamaterials and electromagnetic sources: Tailoring the radiation phase pattern. *Phys. Rev. B* **75,** 155410 (2007).
19. Li, Y. *et al.* On-chip zero-index metamaterials. *Nat. Photonics* **9,** 738–742 (2015).
20. Bravo-Abad, J., Joannopoulos, J. D. & Soljačić, M. Enabling single-mode behavior over large areas with photonic Dirac cones. *Proc. Natl. Acad. Sci.* **109,** 9761–9765 (2012).
21. Lu, L., Fu, L., Joannopoulos, J. D. & Soljačić, M. Weyl points and line nodes in gyroid photonic crystals. *Nat. Photonics* **7,** 294–299 (2013).
22. Lu, L. *et al.* Experimental observation of Weyl points. *Science* **349,** 622–624 (2015).
23. Haldane, F. D. M. & Raghu, S. Possible Realization of Directional Optical Waveguides in Photonic Crystals with Broken Time-Reversal Symmetry. *Phys. Rev. Lett.* **100,** 13904 (2008).
24. Wang, Z., Chong, Y. D., Joannopoulos, J. D. & Soljačić, M. Reflection-Free One-Way Edge Modes in a Gyromagnetic Photonic Crystal. *Phys. Rev. Lett.* **100,** 13905 (2008).
25. Wang, Z., Chong, Y., Joannopoulos, J. D. & Soljacic, M. Observation of unidirectional backscattering-immune topological electromagnetic states. *Nature* **461,** 772–775 (2009).

26. Wu, L.-H. & Hu, X. Scheme for Achieving a Topological Photonic Crystal by Using Dielectric Material. *Phys. Rev. Lett.* **114,** 223901 (2015).
27. Ma, T. & Shvets, G. All-Si valley-Hall photonic topological insulator. *New J. Phys.* **18,** 25012 (2016).
28. Castro Neto, A. H., Guinea, F., Peres, N. M. R., Novoselov, K. S. & Geim, A. K. The electronic properties of graphene. *Rev. Mod. Phys.* **81,** 109–162 (2009).
29. Johnson, S. G. & Joannopoulos, J. D. Block-iterative frequency-domain methods for Maxwell's equations in a planewave basis. *Opt. Express* **8,** 173 (2001).
30. Wang, Y. *et al.* Design of broadband subwavelength grating couplers with low back reflection. *Opt. Lett.* **40,** 4647 (2015).
31. Fan, S. & Joannopoulos, J. D. Analysis of guided resonances in photonic crystal slabs. *Phys. Rev. B* **65,** 235112 (2002).
32. Joannopoulos, J. D., Johnson, S. G., Winn, J. N. & Meade, R. D. *Photonic Crystals: Molding the Flow of Light*. (Princeton University Press, 2008).
33. Chrostowski, L. & Hochberg, M. *Silicon Photonics Design: From Devices to Systems*. (Cambridge University Press, 2015).
34. Jukić, D., Buljan, H., Lee, D.-H., Joannopoulos, J. D. & Soljačić, M. Flat photonic surface bands pinned between Dirac points. *Opt. Lett.* **37,** 5262 (2012).
35. Hirose, K. *et al.* Watt-class high-power, high-beam-quality photonic-crystal lasers. *Nat. Photonics* **8,** 406–411 (2014).
36. Klitzing, K. v., Dorda, G. & Pepper, M. New Method for High-Accuracy Determination of the Fine-Structure Constant Based on Quantized Hall Resistance. *Phys. Rev. Lett.* **45,** 494–497 (1980).

37. Guinea, F., Katsnelson, M. I. & Geim, A. K. Energy gaps and a zero-field quantum Hall effect in graphene by strain engineering. *Nat Phys* **6,** 30–33 (2010).

38. Levy, N. *et al.* Strain-Induced Pseudo–Magnetic Fields Greater Than 300 Tesla in Graphene Nanobubbles. *Science* **329,** 544–547 (2010).

39. Englund, D. *et al.* Controlling the Spontaneous Emission Rate of Single Quantum Dots in a Two-Dimensional Photonic Crystal. *Phys. Rev. Lett.* **95,** 13904 (2005).

40. Soljacic, M. & Joannopoulos, J. D. Enhancement of nonlinear effects using photonic crystals. *Nat. Mater.* **3,** 211–219 (2004).

41. Moitra, P. *et al.* Realization of an all-dielectric zero-index optical metamaterial. *Nat. Photonics* **7,** 791–795 (2013).

42. Haldane, F. D. M. Model for a Quantum Hall Effect without Landau Levels: Condensed-Matter Realization of the 'Parity Anomaly'. *Phys. Rev. Lett.* **61,** 2015–2018 (1988).

43. König, M. *et al.* Quantum Spin Hall Insulator State in HgTe Quantum Wells. *Science* **318,** 766–770 (2007).

44. Chang, C.-Z. *et al.* Experimental Observation of the Quantum Anomalous Hall Effect in a Magnetic Topological Insulator. *Science* **340,** 167–170 (2013).

45. Jotzu, G. *et al.* Experimental realization of the topological Haldane model with ultracold fermions. *Nature* **515,** 237–240 (2014).

46. Khanikaev, A. B. *et al.* Photonic topological insulators. *Nat. Mater.* **12,** 233–239 (2013).

47. Cheng, X. *et al.* Robust reconfigurable electromagnetic pathways within a photonic topological insulator. *Nat. Mater.* **15,** 542–548 (2016).

48. Fang, K., Yu, Z. & Fan, S. Realizing effective magnetic field for photons by controlling the phase of dynamic modulation. *Nat. Photonics* **6,** 782–787 (2012).